University of Baghdad
College of Engineering
JE
JOURNAL OF ENGINEERING

Journal of Engineering

journal homepage: www.jcoeng.edu.iq

Volume 32 Number 6 June 2026

Influence of Fly Ash Incorporation and Thermal Curing on the Performance of Reactive Powder Concrete

Nadia Salman Hussein *, Hadeel K. Awad

Department of Civil Engineering, College of Engineering, University of Baghdad, Baghdad, Iraq

ABSTRACT

The primary objective of this study is to investigate the effects of thermal curing and fly ash incorporation on the mechanical and physical properties of reactive powder concrete (RPC) to develop a more sustainable RPC mixture with partial replacement of ordinary Portland cement (OPC) by fly ash. Four mixes were prepared: a reference mix (R) and mixes with fly ash replacement levels of 10%, 20%, and 30% (RF10, RF20, and RF30). Each mixture was cast and tested in three specimens for each age of testing. The specimens were thermally cured at 70°C for 5 hours per day for a total of 3 days, followed by water curing until the testing age. The experiments showed that adding 20% fly ash improved the overall performance of RPC. The RF20 mix showed the best compressive strength, with increases of 3.39%, 4.47%, and 4.86% at 7, 28, and 56 days, respectively, relative to a reference mix. Furthermore, flexural strength and splitting tensile strength increased by 2.39% and 1.69%, respectively, at 28days. The RF20 mixture had the highest dry density (2683 kg/m^3), the lowest water absorption (0.114%), and the lowest porosity (1.75%). However, a 30% replacement of cement with fly ash reduced mechanical properties. Results indicated that 20% fly ash inclusion under thermal curing conditions could effectively improve RPC performance and promote sustainability by reducing cement use.

Keywords: Curing regime, Fly ash, Mechanical properties, Reactive powder concrete, Steel fibers, Thermal curing.

1. INTRODUCTION

The Technology of concrete is advancing rapidly. A new material found was Reactive Powder Concrete (RPC). RPC is used in the best of construction at a lower cost and can build infinitely stronger, more durable structures. **(Nafees et al., 2021; Aboud et al., 2019; Majeed et al., 2023).** RPC is formed from very fine powders, such as Portland cement, sand, silica fume, and quartz powder. RPC is characterized by a very low water-to-cement (W/C) ratio, and superplasticizers are also used to enhance the workability. Steel fibers are sometimes added

*Corresponding author
Peer review under the responsibility of University of Baghdad.
https://doi.org/10.31026/j.eng.2026.06.05

Article received: 13/04/2026
Article revised: 25/05/2026
Article accepted: 27/05/2026
Article published: 01/06/2026

(Danha et al., 2013; Soutsos et al., 2006). Although RPC exhibits excellent performance compared to normal concrete, it is also brittle under tensile and compressive loading; thus, to improve its toughness and post-cracking behavior, fiber reinforcement is commonly used **(Muhsin and Fawzi, 2021; Xu et al., 2016).** Fly ash is produced when pulverized structures of coal are burned to produce electricity. Exhaust gases carry mineral impurities, such as shale, quartz, feldspar, and clay, into suspension after they are burned. Fly ash is the glassy particles formed from the cooling and hardening of fused materials. Electrostatic precipitators and bag filters are employed to collect the finely divided fly ash, while the combustion products form a fine powder. However, much of this waste is produced each year, posing a real threat to the environment **(Nayak et al., 2022).** It diminishes the hydration temperature. As working properties improve, the amount of water needed decreases. Such concrete can be less permeable and more resistant to sulfate attack. It solves the cracking issue seen in Portland cement. Mixing fly ash into concrete decreases CO_2 emissions and, thus, is commonly considered an environmentally beneficial application of solid waste **(Kamara et al., 2023).** Strength gain is beneficial due to the pozzolanic reaction, and a properly developed microstructure of cement paste can be important **(Ahmad, 2022; Shannag and Yeginobali, 1995; Shannag, 2000).** The enhancement has been attributed to the fineness of the particles, as they react with the cement silicate hydration products [$Ca(OH)_2$] to form a higher-quality gel **(Thomas, 2007).**

(Yazıcı et al., 2009) explored the viability of developing low-cement reactive powder concrete (RPC) in which cement is replaced with fly ash (FA), namely Class C FA, up to 60%. The study used standard water curing, steam curing, and autoclave curing of specimens, prepared two different RPC series with bauxite and granite aggregates, and evaluated different mechanical properties. The results showed that high-volume fly ash RPC had compressive strengths of up to 200 MPa; thermal curing led to compressive strengths of up to 250 MPa; and applying external pressure during the setting and hardening phases resulted in compressive strengths of up to 400 MPa. **(Gamal et al., 2019)** examined RPC using fly ash (FA) as a partial cement replacement, including 25% FA and combinations of 15%, 20%, and 25% FA with a constant 10% silica fume. Slump flow, compressive strength, flexural strength, splitting tensile strength, and density of the mixes were tested after curing at 25 °C, 60 °C, and 90 °C.

The results revealed that compressive strength increases with temperature, reaching a peak of 149.1 MPa after 1 day at 90 °C. **(Muhsin and Fawzi, 2021)** investigated sustainable RPC using fly ash as a partial cement substitute (8, 12, and 16%) with a binder content of 800kg/m^3 (w/b ratio of 0.275) and micro steel fibers at 1%. Mechanical properties were assessed at 7, 28, and 90 days. The best results were obtained with 8% fly ash, where compressive, tensile, and density strengths were 96.5 MPa, 9.38 MPa, and 2395 kg/m^3, respectively. Moreover, the results show that fly ash performs well on RPC mechanical performance and contributes to sustainability. **(Rahul, 2023)** also intends to propose a green RPC by partially substituting cement with pozzolanic industrial supplementary materials. At 30% replacement of cement, the uppermost strength was achieved, for which pozzolanic materials can enhance RPC performance. **(Safitri et al., 2024)** studied the effect of fly ash as a partial replacement of cement in RPC with substitution levels of 0%, 5%, 10%, 15%, 20%, and 25%, keeping Quartz Sand constant at 30%, was studied. High-strength concrete was produced for all mixes, with a compressive strength of 75.59 MPa observed at 10% fly ash content, indicating an improvement in compressive strength.

Although Previous studies have shown that incorporating fly ash and thermal curing improves the performance of RPC. However, most studies focused mainly on compressive strength or used different curing regimes, material compositions, and replacement levels. Also, a few studies have been conducted on the combined effect of fly ash replacement and controlled thermal curing at 70 °C on the physical and mechanical properties of RPC. Therefore, the objective of the present study is to determine the optimum fly ash replacement level under controlled thermal curing conditions at 70 ^{o}C by evaluating density, water absorption, porosity, compressive strength, flexural strength, and splitting tensile strength to provide a more comprehensive understanding of RPC performance and sustainability.

2. MATERIALS AND METHOD

2.1 Materials

2.1.1 Fly Ash

Fly Ash was categorized as Class F, and the standards were established in accordance to **(ASTM C618-25a, 2025). Tables 1 and 2** present the chemical and physical properties.

Table 1. Chemical composition of fly ash.

Chemical composition	Results %	(ASTM C618-25a, 2025) Class F Requirement
Fe_2O_3	5.20	sum of value more than 50%
Al_2O_3	17.75	
SiO_2	65.57	
SO_3	0.26	Maximum 5%
MgO	0.86	---
CaO	2.2	Max 18%
K2O	3.40	---
Na_2O	2.25	---
Loss of ignition (L.O.I)	2.8	Max 6%

Table 2. Physical characteristics of fly ash.

Physical properties	Results %	(ASTM C618-25a, 2025) class F Requirement
Maximum amount retained at 45µm (No. 325) sieve: 34%	26.8	Max 34%
Specific gravity	2.330	----
Surface area (Blaine method) cm^2/ g	6100	----
Physical form	powder	----
Strength Activity Index with Portland cement at 7 days	97	min 75

2.1.2 Cement

The OPC (CEM 1-42.5 R) cement used in the studies meets the chemical and physical characteristics outlined in **(IQS No. 5, 2019)**. **Tables 3** and **4** present the properties of cement.

2.1.3 Sand

Fine aggregate that passed through a 600μm sieve. Normal specifications for fine aggregate were met. **(IQS No.45, 1984).** The fine aggregate properties shown in **Tables 5** and **6** show the sand grading.

Table 3. The physical properties of the cement.

Physical properties		**Results%**	**Limits of (IQS. No.5, 2019)**
Specific surface area (Blaine approach) (m^2/kg)		402.6	≥ 280
Setting time (Vicat's approach) Initial setting (min)		110	≥ 45 min
Setting time (Vicat's approach) Final setting time (hr)		3.25	≤ 10 hr.
Soundness by Autoclave Approach (%)		0.036	≤ 0.80
Compressive strength (MPa)	(2) days	23.3	≥20
	(28) days	43	≥ 42.5

Table 4. Chemical composition of the cement.

Oxide Compositions	**Weight (%)**	**Limits of (IQS. No.5, 2019)**
L.O. I	2.815	Max (4)
Lime (CaO)	63.89	-----
Iron oxide (Fe_2O_3)	3.58	-----
Alumina (Al_2O_3)	5.40	-----
Silica (SiO_2)	18.87	-----
Magnesia (MgO)	1.84	Max (5)
Sulfate (SO_3)	2.33	SO_3≤ 2.8 if C_3A > 3.5 SO_3≤ 2.5 if C_3A ≤ 3.5
Insoluble residue (IR)	0.51	Max (1.5)
Cl^- (Chloride)	0.078	—
Major compounds of OPC		
Tri-calcium Silicate (C_3S)	68.64	Bogue equation calculation using equations according to **(ASTM C150/150M -24, 2024)**
Di-calcium Silicate (C_2S)	2.32	
Tri-calcium Aluminate (C_3A)	8.25	
Tetra-calcium Aluminoferrite (C_4AF)	10.89	

Table 5. Grading of fine aggregate.

Sieve size (mm)	**Cumulative Passing %**	**Limits according to (IQS No.45, 1984)– Zone 4**
10	100	100
4.75	100	95-100
2.36	100	95-100
1.18	100	90-100
0.6	100	80-100
0.3	28.1	15-50
0.15	5.4	0-15

Table 6. Physical and chemical characteristics of fine aggregates.

Properties	Test results	(IQS No.45, 1984)
Specific gravity	2.56	------
Material Finer than 0.075 mm (%)	2.5	Max (5)
Fineness modulus	1.67	------
Dry rodded density (kg/m^3)	1680	------
Absorption (%)	1.07	------
Sulfate content %	0.18	Max (0.5)

2.1.4 Silica Fume

The properties and strength activity index of silica fume meet the requirements of **(ASTM C1240-20, 2020)**, their chemical and physical characteristics are shown in **Tables 7** and **8.**

Table 7. Chemical composition of Silica Fume (SF).

Oxide	Results %	(ASTM C1240-20, 2020), requirement
Silicon Oxide (SiO_2)	92.23	Min (85) %
Aluminum Oxide (Al_2O_3)	0.31	------
Magnesium Oxide (MgO)	0.34	------
Iron Oxide (Fe_2O_3)	1.3	------
Calcium Oxide (CaO)	2.8	------
Loss of Ignition	2.13	Max (6) %
Moisture content	0.32	Max (3) %

Table 8. Physical requirements of Silica Fume (SF).

Physical properties	Test results	(ASTM C1240-20, 2020), requirement
State	Amorphous powder with submicron particle size	-
Color	Gray to medium gray powder	-
Retained on 45 µ (No.325) sieve (%)	7.1	≤ (10)
Accelerated Pozzolanic Strength Activities Index with the OPC at 7 days, min percent of control	111.4	≥ (105)

2.1.5 Water

Tap water for mixing and curing is suitable **(IQS No.1703, 2018)**.

2.1.6 Superplasticizer

Hyperplast PC800M-type G (water-reducing, high-range, and retarding admixtures) have a density of 1.070 ± 0.02 g/cm^3. The superplasticizer was used at a dosage of 0.5 - 3.5 % by weight of the total cementitious materials and having a pH of (5–7), in compliance with **(ASTM C494/C494M-24, 2024)**.

2.1.7 Micro Steel Fiber

A straight micro steel fiber with a nominal diameter of 0.2 mm and length of 13 mm was employed in this study, providing an aspect ratio for the fiber length to diameter (l/d) =65 and density 7860 kg/m^3. Tensile Strength 2600 MPa as presented in **Fig. 1**

2.2 Design and Mixes

The mixtures were prepared as described by **(Richard and Cheyrezy, 1995; Hussain and Aljalawi, 2022).** The mixtures were: a control (R) with 100% cement, and three sustainable mixtures with 10%, 20%, and 30% of the cement weight substituted by fly ash, named RF10, RF20, and RF30, respectively. All compositions were developed based on a constant water-to-cementitious materials ratio (w/cm) of 0.21 and silica fume 25% by weight of cement, as shown in **Fig. 1**. The selected materials are presented. A superplasticizer dosage ranging from 1.75–1.9% by weight of the total cementitious materials was used to achieve the required workability. The flowability was adjusted by the flow table test according to **(ASTM C1437-20, 2020),** resulting in a value of (110 ± 5 mm) indicated by **(ASTM C109/C109M-24, 2024)**. The control and another RPC mixture's flow values ranged from 110 mm to 115 mm, as presented in **Fig. 2**. **Table 9** summarizes the proportions of the mixtures.

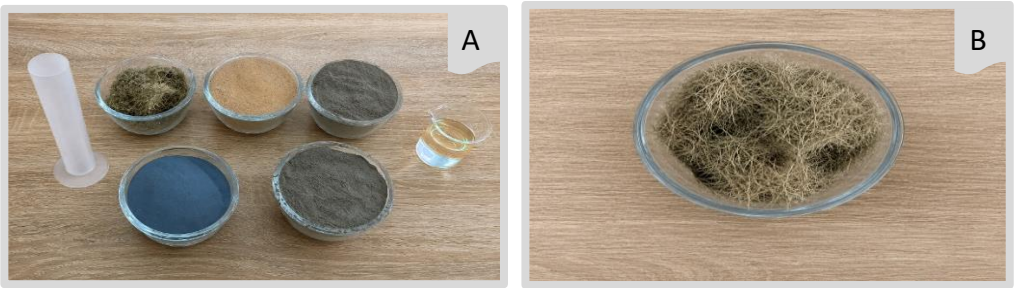

Figure 1. Raw materials **(A)** and micro steel fibers **(B)** used in the RPC mixtures.

Figure 2. Flow table test: **(A)** before flow, **(B)** after flow, and **(C)** diameter measurement.

Table 9. Mix proportions of RPC for 1 m^3 (kg/m^3).

Mixes	Cement	Sand	Silica Fume	Fly Ash	W/Cm Ratio	Water	Sp Cementitious-materials	MicroSteel fiber	Micro Steel fiber%
R	920	1015	230	-------	0.21	242	21.85	78.60	1%
RF10	828			92			21.28		
RF20	736			184			20.70		
RF30	644			276			20.13		

2.3 Mixing and Casting

The mixing procedure was carried out following the method proposed by **(Danha et al., 2013)**. The cement, fly ash, and silica fume were first dry-mixed for 3 minutes before mixing (homogenous distribution). Then 5 minutes of mixing, after adding and incorporating the sand. A little water was used to dissolve the superplasticizer, which was then gradually added to the water-superplasticizer solution during mixing; the mix was then run for 3 min. Portions that the mixer could not reach continued to be mixed by hand. The mixer was subsequently run for an additional 5 min until satisfactory fluidity was reached. Micro steel and glass fibers were uniformly introduced into the mix after 3 min, followed by an additional 2 min of mixing. It takes about 15 minutes overall, from adding water to a given batch to mixing.

2.4 Curing

The normal curing of RPC results in a slower rate of strength development than that observed with heat or steam curing, in which temperature is the main controlling factor **(Luti and Abbas, 2024)**. The new concrete was poured into steel forms immediately after mixing, compacted by vibration, and then covered with nylon sheets. which were demolded after 24 h; specimens were cured in water following a heat-curing regime: increased from 20 °C to 70 °C within the first hour and held at 70 °C for 5 h/day for three consecutive days. Finally, their curing has continued in water at room temperature until the time for testing. The thermal curing regime used was based on **(Khreef and Abbas, 2021)** and complied with **(ACI 517.2R-92, 2017)**. Thermal curing at 70°C was chosen to accelerate the hydration and pozzolanic reactions, which improved the early-age strength development of RPC. **Figs. 3 and 4** illustrate the adopted thermal curing process.

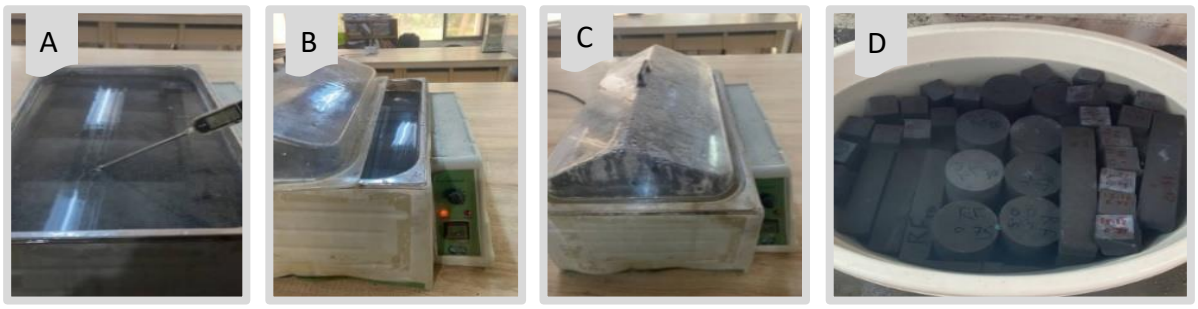

Figure 3. Thermal curing process**: (A)** initial heating stage, **(B)** raising the temperature to 70°C, **(C)** maintaining the specimens at 70°C for 5 h, and **(D)** normal water curing

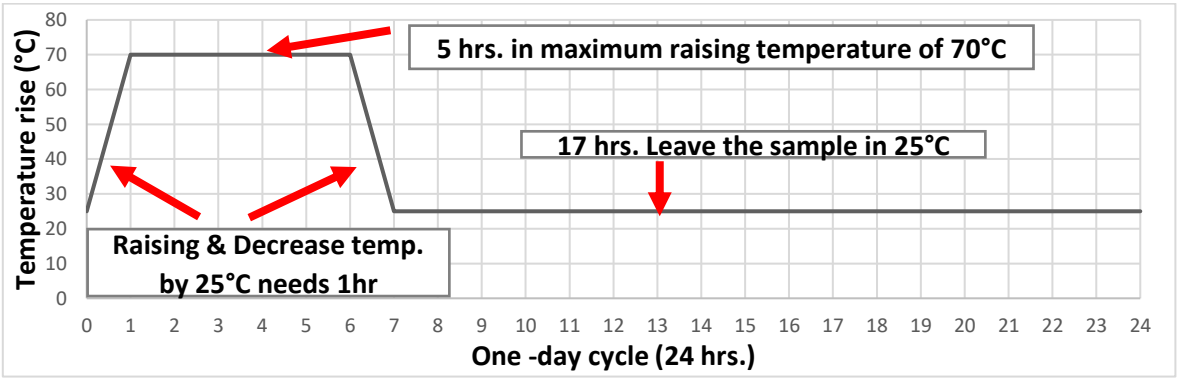

Figure 4. Thermal curing regime for RPC over 24 hours.

2.5 Testing Program

2.5.1 Fresh Density Test

Fresh density of RPC is determined in accordance with **(ASTM C138/C138M-17a, 2017)**, using a known-mass-and-volume cylinder. The fresh density was calculated based on Eq. (1).

$$D_f = \frac{M_c - M_m}{V_m} \quad (1)$$

where: D_f is the fresh density of concrete (kg/m^3), M_c is the mass of the cylinder filled with fresh concrete (kg), M_m is the mass of the empty cylinder (kg), and V_m is the volume of the cylinder (m^3).

2.5.2 Compressive Strength

The compressive strength of RPC (50 × 50 × 50) mm was determined in accordance with **(ASTM C109/C109M, 2020; Abellan-Garcia et al., 2023)** using three cube specimens cured for 7,28 and 56 days. The reported compressive strength values are averages of the three specimens tested at each age. Compressive strength was calculated using Eq. (2), as shown in **Fig. 5**

$$fc = \frac{P}{Ac} \quad (2)$$

where: fc: Compressive Strength (MPa), P: Maximum failure load (N), Ac: Cross-section area (mm^2).

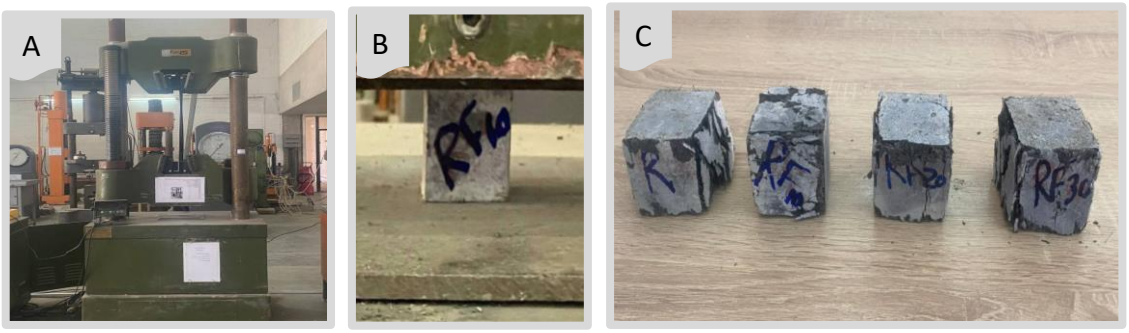

Figure 5. Compression test: **(A)** testing machine, **(B)** loading, and **(C)** failed specimens.

2.5.3 Flexural Strength

Three prismatic specimens (50 × 50 × 250) mm according to the specifications presented in **(ASTM C293/C293M, 2019)**. were tested at curing ages of 7,28 and 56days. Values reported for flexural strength are average test results of three specimens at each age. The flexural strength was determined with Eq. (3), as shown in **Fig. 6**.

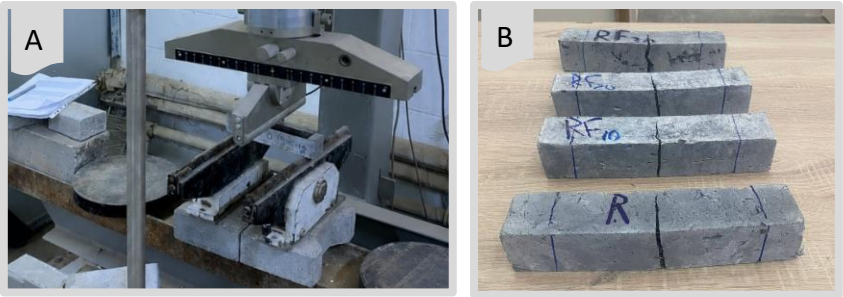

Figure 6. Flexural strength: **(A)** testing machine and **(B)** failed specimens

$$fr = \frac{3pl}{2bd^2} \quad (3)$$

Where: fr -The flexural value is denoted by the letter (MPa), P -Maximum load is denoted by (N), L- stands for the span's length (mm), b -average width of specimen (mm), d -stands for the average prism thickness depth (mm).

2.5.4 Splitting Tensile Test

The splitting tensile strength was determined using cylindrical samples (100 mm in diameter and 200 mm in height). According to **(ASTM C496/C496M, 2017),** with dimensions at the curing ages of 7,28 and 56days. The RPC was tested on three cylindrical specimens. Except where specified, values reported are the average of three specimens per age. Eq. (4), shown in **Fig. 7**.

$$ft = \frac{2p}{\pi dl} \quad (4)$$

where: ft- Indirect tensile strength (MPa), p- Max. Applied load indicated by the testing machine (N), d-Cylinder diameter (mm), l-Cylinder length (mm).

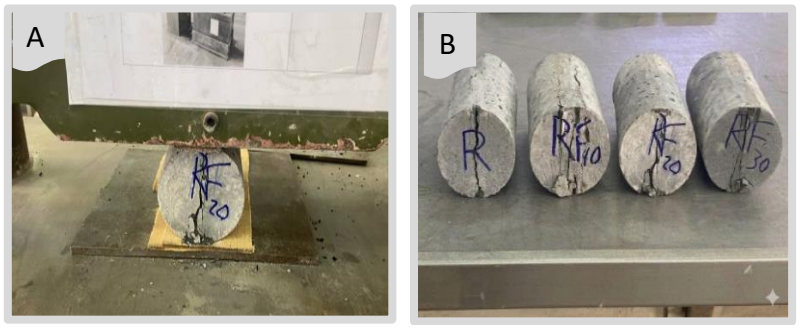

Figure 7. Splitting tensile test **(A)** testing machine and **(B)** failed specimens

2.5.5 Bulk Dry Density Test

Density was tested per **(ASTM C642-21, 2021)**. Three (50 × 50 × 50) mm cubes were tested in 28 days. was consulted for the test. RPC Density formula Eq. (5).

$$D = \frac{A}{B-C} * \rho \quad (5)$$

where: D = density of specimen (kg/m^3), A = weight of oven-dried sample in air (g). B =weight of surface-dry sample in air after immersion and boiling (g). C = Apparent weight of surface-dry sample in air after immersion and boiling (g). ρ= Density of water, (kg/m^3).

2.5.6 Water Absorption and Voids Test

Water absorption and voids tests were conducted 28 days following **(ASTM C642-21, 2021)**. computed from the mean of three specimens. The water absorption ratio was calculated using Eq. (6), and the void content was calculated using Eq. (7).

$$Absorption\% = \frac{B-A}{A} * 100 \quad (6)$$

Where: A=Oven dry weight (g), B=Saturated surface dry weight (g).

$$\text{Voids}\% = \frac{W2-W1}{W2-W3} \quad (7)$$

Where: W1: The sample mass is oven-dried in the air, W2: The mass of the sample is surface dried in the air after being submerged in water, and W3: The mass of the sample in the water

3. RESULTS AND DISCUSSION

3.1 Dry and Fresh Density

Fresh and dry densities of 28 days are given in **Table 10** and **Fig. 8**. A slight decrease in fresh density was observed with increasing fly ash content. However, this can be because of the low specific gravity of fly ash compared to that of cement, which increases paste volume but decreases the total mass of the mixture **(Huy et al., 2017)**.On the other hand, the dry density was increased as RF10 and RF20 due to the filling effect of fly ash grains in addition to the pozzolanic reaction between the calcium hydroxide and fly ash (during the hydration process) that may lead to the formation of extra amorphous C–S–H gel and decrease the porosity **(Muhsen and Fawzi, 2021)**.

Table 10. Results of Fresh and Dry Density

Mixes	Fresh (kg/m^3)	Dry at 28 days (kg/m^3)
R	2515	2645
RF10	2512	2652
RF20	2506	2683
RF30	2498	2638

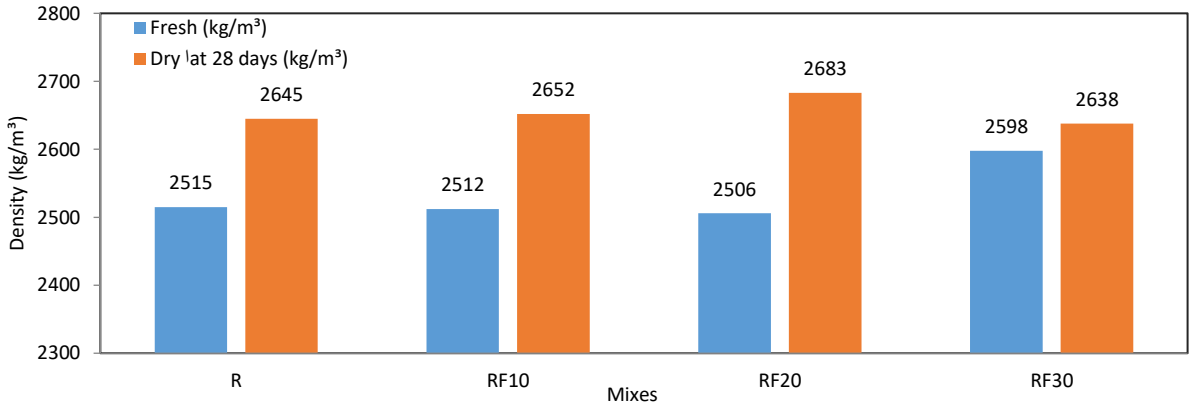

Figure 8. Fresh and Dry density of reference and RPC mixes.

However, the decrease in dry density at higher replacement levels (RF30) at 28 days may be attributed to the limited availability of calcium hydroxide required to complete the effective pozzolanic reactions **(Nayak et al., 2022).** Overall, the results suggest that moderate fly ash contents (10% and 20%) may improve the microstructural characteristics and density of RPC; however, excessive fly ash replacement may negatively affect RPC densification.

3.2 Water Absorption and Porosity

Table 11 and **Fig. 9** show that water absorption and porosity of the mixtures decreased with the replacement of 20% fly ash. The values decreased from 0·124% and 1·90% (for control mixture(R)) to 0·118% and 1·82% (for RF10), then decreased to 0·114% and 1·75% (for RF20)

However, increasing the replacement level (RF30) led to a higher water absorption and porosity of 0.131% and 1.98%, respectively. The reduced water absorption and porosity resulting from fly ash addition are due to its involvement in a pozzolanic reaction, which may contribute to the formation of additional C–S–H gel and possible matrix densification. This may lead to reduced pore volume and interconnectivity of voids, thereby reducing water sorption capacity **(Papp et al., 2024)**. Moreover, a part of the fly ash acted as a filler, filling the macroscopically observed spacing voids, which may contribute to reducing the size and total porosity of pozzolanic hydrates. However, at higher replacement levels, the reduced amount of cement hydration products may limit the pozzolanic reaction. At the same time, some fly ash particles may remain unreacted and act as inert materials, thereby contributing to increased internal voids and, consequently, increased porosity and water absorption **(Huynh et al., 2024)**.

Table 11. Results of Water absorption and porosity.

Mixes	Water absorption %	Porosity %
R	0.124	1.90
RF10	0.118	1.82
RF20	0.114	1.75
RF30	0.131	1.98

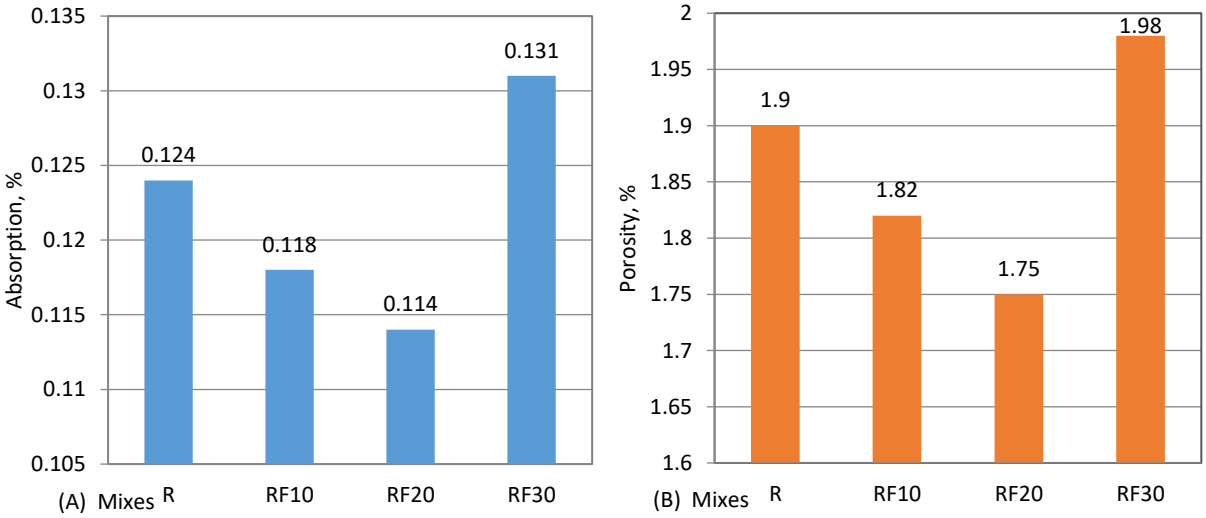

Figure 9. **(A)** Water absorption, and **(B)** porosity of RPC mixtures

3.3 Compressive Strength

The compressive strength of 28 days of RF10 and RF20 increased by 2.81 % and 4.47%, respectively. However, at a higher fly ash replacement level (RF30), the compressive strength reduced by 2.63% in 28 days. The enhanced performance at moderate replacement levels is attributed to the pozzolanic activity and microfiller effect of fly ash, leading to a denser microstructure and improved matrix compactness. Although pozzolanic reactions are slower than hydraulic reactions, early strength may be improved under heat curing because the calcium hydroxide present in the concrete reacts to form additional calcium silicate hydrate (C–S–H) gel **(Thomas, 2007)**. Heat curing accelerated pozzolanic reactions more significantly than hydraulic reactions, leading to improved early-age strength development. In addition, the calcium content of fly ash significantly affects early strength **(Dong et al., 2020).** This behavior could also be enhanced under thermal curing conditions, which may accelerate pozzolanic reactions as illustrated in **Table 12** and **Fig. 10.**

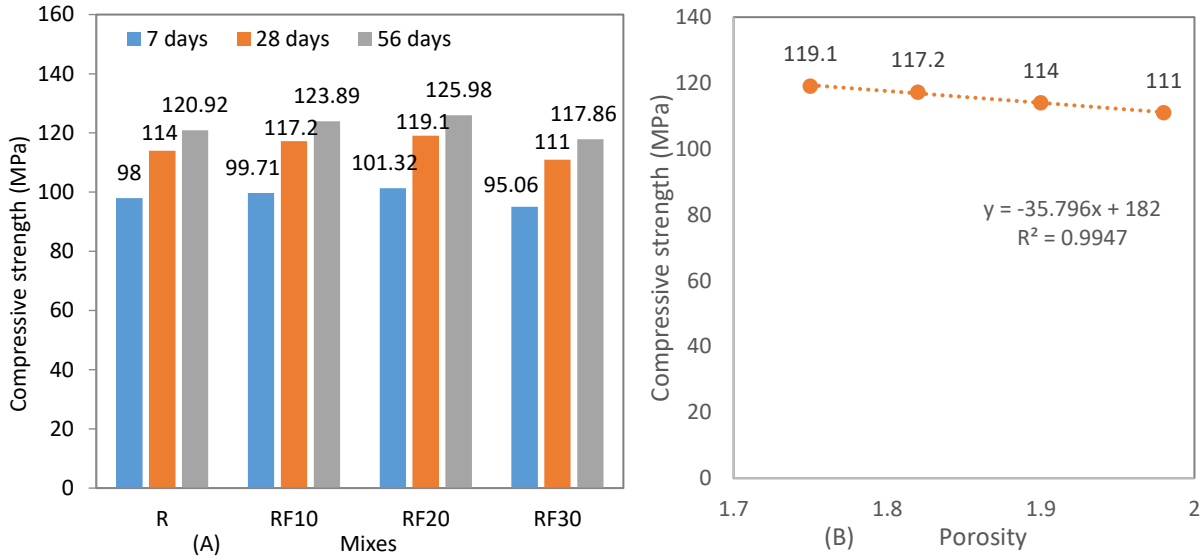

Figure 10. (A) Compressive strength and **(B)** porosity-strength relationship.

Table 12. Results of compressive.

Mixes	Compressive Strength (MPa)			Standard Deviation			Coefficient of Variation (%)			Percentage change relative to reference mix (R)		
	7 days	28 days	56 days	7 days	28 days	56 days	7 days	28 days	56 days	7 days	28 days	56 days
R	98.00	114.00	120.92	1.410	1.410	1.47	1.44	1.24	1.22	0.00	0.00	0.00
RF10	99.71	117.20	124.80	1.56	1.56	1.65	1.56	1.33	1.32	+1.74	+2.81	+3.21
RF20	101.32	119.10	126.80	1.457	1.374	1.6	1.44	1.15	1.26	+3.39	+4.47	+4.86
RF30	95.06	111.00	117.86	1.5	1.8	1.55	1.58	1.62	1.31	−3.00	−2.63	−2.53

3.4 Flexural Strength

The flexural strength improved with fly ash replacement up to 20% at all ages compared to the control mixture. The strength increased by +1.15% and +2.39% in 28 days for RF10 and

RF20, respectively. This improvement may be attributed to the pozzolanic reactions of fly ash and silica which promoted the formation of additional formation of additional C–S–H gel. This may contribute to a denser and less porous interfacial transition zone **(Yazıcı et al., 2008)**. In addition, the presence of uniformly distributed fibers may improve the bond between the matrix and fibers, thereby enhancing resistance to tensile stresses under flexural loading. **(Al-Louh, 2014)** reported similar observations. At higher replacement levels (RF30), the reduced pozzolanic reaction due to a less dense matrix may result in lower flexural strength. In general, moderate replacement with fly ash (10–20%) may improve flexural performance, whereas excessive replacement may negatively affect strength, as illustrated in **Fig. 11** and **Table 13**.

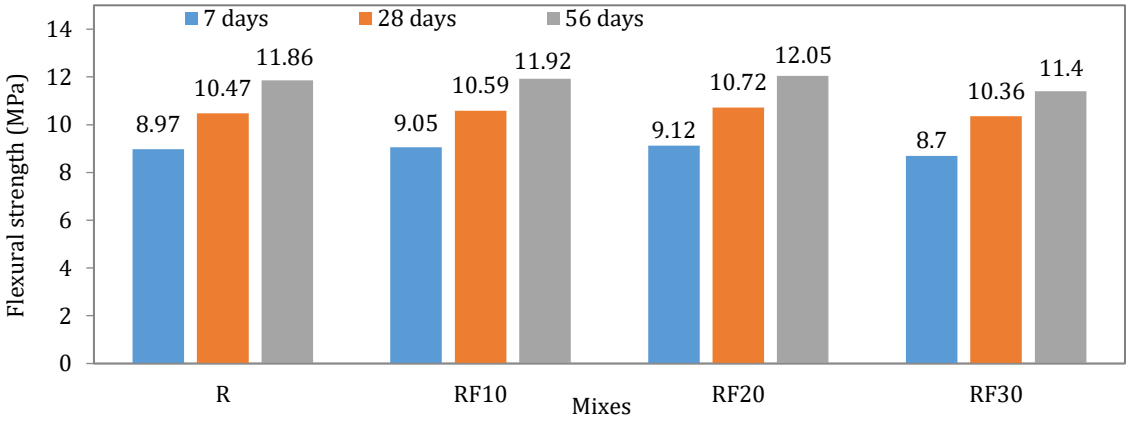

Figure 11. Effect of fly ash on the flexural strength of RPC mixtures

Table 13. Results of Flexural Strength

Mixes	Flexural strength (MPa)			Standard Deviation			Coefficient of Variation (%)			Percentage change relative to reference mix (R)		
	7 days	28 days	56 days	7 days	28 days	56 days	7 days	28 days	56 days	7 days	28 days	56 days
R	8.97	10.47	11.86	0.157	0.157	0.175	1.75	1.5	1.48	0.00	0.00	0.00
RF10	9.05	10.59	11.92	0.136	0.160	0.180	1.51	1.51	1.51	+0.89	+1.15	+1.60
RF20	9.12	10.72	12.05	0.157	0.157	0.195	1.72	1.47	1.62	+1.67	+2.39	+2.87
RF30	8.80	10.29	11.69	0.141	0.165	0.185	1.61	1.61	1.59	−1.95	−1.70	−1.45

3.5 Splitting Tensile Strength Test

The splitting tensile strength also increased with increasing fly ash content up to 20%, suggesting that hydration and pozzolanic reactions contributed to pore refinement and reduced porosity. For RF10 and RF20, the strengths at 28 days increased by +1.12% and +1.69%, respectively. This improvement may be attributed to fly ash. The hydration process may continue due to pozzolanic reactions. This increase may also be attributed to the pozzolanic activity of fly ash, which can reduce porosity and improve tensile strength. **(Muhsin and Fawzi, 2021)**. The decrease in tensile strength at higher replacement levels (RF30) can be attributed to the limited availability of calcium hydroxide, which was insufficient for pozzolanic reactions. In general, the optimal fly ash content increases tensile strength, whereas a high replacement level may lead to poor performance, as shown in **Table 14** and **Fig. 12.**

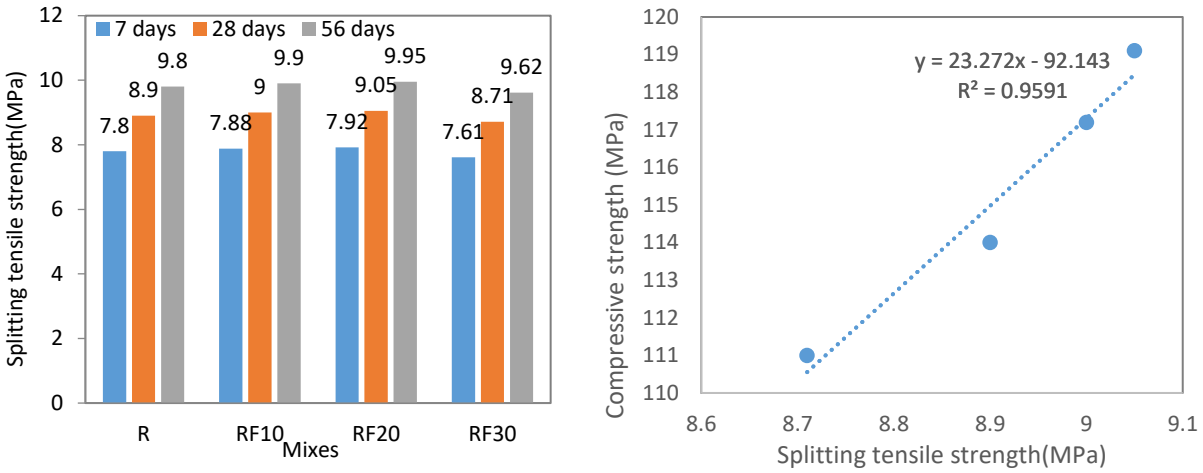

Figure 12. (A) Splitting tensile strength and **(B)** tensile-compressive strength relationship

Table 14. Results of splitting tensile strength.

Mixes	Splitting tensile strength (MPa)			Standard Deviation			Coefficient of Variation (%)			Percentage change relative to reference mix (R)		
	7 days	28 days	56 days	7 days	28 days	56 days	7 days	28 days	56 days	7 days	28 days	56 days
R	7.80	8.90	9.80	0.132	0.132	0.142	1.7	1.49	1.45	0.00	0.00	0.00
RF10	7.88	9.00	9.90	0.115	0.135	0.145	1.47	1.51	1.47	+1.03	+1.12	+1.22
RF20	7.92	9.05	9.95	0.157	0.132	0.142	1.98	1.46	1.43	+1.54	+1.69	+1.84
RF30	7.61	8.71	9.62	0.105	0.125	0.135	1.39	1.44	1.41	−2.45	−2.10	−1.85

Statistical analysis indicated that all tested mixes had low coefficients of variation (COV) values ranging from 1.15% to 1.98%. These values for laboratory trial batches were in the "Excellent" category according to **(ACI Committee 214R-11, 2011)**, implying good uniformity and repeatability of the experimental results. The slight variation observed among the replicate specimens confirms the reliability of the adopted mixing, casting, curing, and testing procedures. Also, the small standard deviations indicate that the measured results were close to the mean values, indicating stable behavior for the reference and RF mixtures.

4. CONCLUSIONS

Based on the experimental results obtained in this study, the following conclusions can be drawn:

1. As the proportion of fly ash increased, the fresh density decreased slightly. At 10–20% replacement, the dry density increased, reaching a maximum of 2683 kg/m^3 (RF20). A reduction was observed at 30% replacement. This behavior may be attributed to the micro-filler effect and pozzolanic reaction of fly ash, which may contribute to matrix densification under thermal curing conditions.
2. Increasing the fly ash content to 20% decreased water absorption and porosity. The RF20 showed the lowest values of 0.114% and 1.75%, respectively. However, both properties increased at the 30% replacement level. The reduction in absorption and

porosity at moderate replacement levels may be associated with pore refinement and the formation of additional C–S–H gel resulting from the pozzolanic activity of fly ash.

3. The addition of fly ash improves compressive strength at 10% and 20%, with RF20 achieving the highest value of 119.10 MPa at 28 days, an increase of 4.47%. At 30% replacement level, the strength decreased. The improvement could be attributed to the improved particle packing density and possible matrix densification promoted by thermal curing and fly ash incorporation.
4. The optimum fly ash replacement level in this study with 20% fly ash, which produced a maximum increase in tensile splitting strength (1.69%) at 28 days for RF20. A decline occurred at 30%. This enhancement may be attributed to improved bonding between the cementitious matrix and fine particles resulting from pozzolanic reactions under thermal curing conditions.
5. Flexural strength improved with fly ash replacement up to 20%, where RF20 recorded the highest increase of 2.39% in 28 days. However, higher replacement levels negatively affected flexural performance. The improvement at moderate fly ash content may be due to matrix densification and reduced internal voids, whereas excessive replacement could lead to insufficient cementitious hydration products.
6. The best replacement of fly ash was 20% (RF20) across all evaluated properties, achieving a balanced performance and improving pore structure characteristics and strength. The results suggest the potential benefits of the combined effect of fly ash incorporation and heat curing on the overall performance of RPC and on the contribution towards a more sustainable cementitious composite.

NOMENCLATURE

Symbol	Description	Symbol	Description
A	Oven-dry mass (g)	OPC	Ordinary Portland cement
Ac	Cross-sectional area (mm^2)	P	Maximum applied load (N)
B	Width of prism (mm)	R	Reference mix (0% fly ash)
B	Saturated surface dry (g)	RF10	RPC with 10% fly ash
D	Dry density (kg/m^3)	RF20	RPC with 20% fly ash
D	Diameter or depth (mm)	RF30	RPC with 30% fly ash
Df	Fresh density (kg/m^3)	RPC	Reactive powder concrete
FA	Fly ash	SF	Silica fume
Fc	Compressive strength (MPa)	SP	Superplasticizer
Fr	Flexural strength (MPa)	V	Volume of specimen (m^3)
Ft	Splitting tensile strength (MPa)	Vm	Volume of cylinder mold (m^3)
L	Span length (mm)	W1	Oven-dry mass of specimen in air (g)
Mc	Mass of cylinder filled with fresh concrete (kg)	W2	Saturated surface dry mass (g)
Mm	Mass of empty cylinder (kg)	W3	Apparent mass of specimen in water (g)

Credit Authorship Contribution Statement

Nadia Salman Hussein: Visualization and draft writing, discussion and linguistic review. Hadeel K. Awad: Conducting and analyzing results and proofreading

Declaration of Competing Interest

The authors declare that they have no known competing financial interests or personal relationships that could have appeared to influence the work reported in this paper.

REFERENCES

Abellan-Garcia, J., Redondo-Mosquera, J., Khan, M.I., Abbas, Y.M. and Castro-Cabeza, A., 2023. Development of a novel 124 MPa strength green reactive powder concrete employing waste glass and locally available cement. *Archives of Civil and Mechanical Engineering*, 23, P. 161. https://doi.org/10.1007/s43452-023-00695-7

Aboud, R.K., Awad, H.K., and Mohammed, S.D., 2019. Fire flame effect on the compressive strength of reactive powder concrete using different methods of cooling. *IOP Conference Series: Materials Science and Engineering,* 518(2), P. 022029. https://doi.org/10.1088/1757-899X/518/2/022029

ACI 517.2R-92, 2017. Accelerated curing of concrete at atmospheric pressure, USA: ACI Committee 517. American Concrete Institute (ACI)

ACI 214R-11, 2011. Guide to evaluation of strength test results of concrete. USA: ACI Committee 214. American Concrete Institute (ACI)

Ahmad, S., Al-Amoudi, O.S., Khan, S.M. and Maslehuddin, M., 2022. Effect of silica fume inclusion on the strength, shrinkage, and durability characteristics of natural pozzolan-based cement concrete. *Case Studies in Construction Materials*, 17, P. e01255. https://doi.org/10.1016/j.cscm.2022.e01255

ASTM C138/C138M-a, 2017. Standard test method for density (unit weight), yield, and air content of concrete. ASTM International

ASTM C496/C496M, 2017. Standard test method for splitting tensile strength of cylindrical concrete specimens. ASTM International

ASTM C293/C293M, 2019. Standard test method for flexural strength of concrete (using simple beam with center-point loading)

ASTM C1240-20, 2020. Standard specification for silica fume used in cementitious mixtures. ASTM International

ASTM C1437-20, 2020. Standard test method for flow of hydraulic cement mortar. ASTM International

ASTM C642-21, 2021. Standard test method for density, absorption, and voids in hardened concrete ASTM International

ASTM C150/C150M-24, 2024. Standard specification for Portland cement. ASTM International

ASTM C494/C494M, 2024. Standard specification for chemical admixtures for concrete. ASTM International

ASTM C618-25a, 2025. Standard specification for coal fly ash and natural pozzolan. ASTM International

Danha, L.S., Khalil, W.I., and Al-Hassani, H.M., 2013. Mechanical properties of reactive powder concrete (RPC) with various steel fiber and silica fume contents. *Engineering and Technology Journal*, 31(16), pp. 3090–3108.

Dong, P.S., Tuan, N.V., Thanh, L.T., Thang, N.C., Cu, V.H., and Mun, J.H., 2020. Compressive strength development of high-volume fly ash ultra-high-performance concrete under heat curing conditions with time. *Applied Sciences*, 10(20), P. 7107. https://doi.org/10.3390/app10207107

El-Louh, O.M., 2014. *Fresh and hardened properties of locally produced reactive powder concrete*. Master's thesis. Islamic University of Gaza.

Gamal, I.K., Elsayed, K.M., Makhlouf, M.H., and Alaa, M., 2019. Properties of reactive powder concrete using local materials and various curing conditions. *European Journal of Engineering Research and Science*, 4(6), pp. 74–80. https://doi.org/10.24018/ejeng.2019.4.6.1370

Hussain, Z.A. and Aljalawi, N.M.F., 2022. Behavior of reactive powder concrete containing recycled glass powder reinforced by steel fiber. *Journal of the Mechanical Behavior of Materials*, 31(1), pp. 25–34. https://doi.org/10.1515/jmbm-2022-0003

Huy, N.S.I., Tam, T.T., and Phuoc, H.T., 2017. Effect of fly ash content on the compressive strength development of concrete. *Journal of Science and Technology in Civil Engineering (STCE)-HUCE*, *2*, pp. 31-36.

Huynh, T.P., Ngo, S.H., and Nguyen, V.D., 2024. A modified reactive powder concrete made with fly ash and river sand: An assessment on engineering properties and microstructure. *Periodica Polytechnica Civil Engineering*. https://doi.org/10.3311/PPci.23912

Kamara, S., Foday, J.R., E.H., and Wang, W., 2023. A review on the utilization and environmental concerns of coal fly ash. *American Journal of Chemical and Pharmaceutical Sciences,* 2(2), pp. 53–65. https://doi.org/10.54536/ajcp.v2i2.1609

Khreef, S.M. and Abbas, Z.K., 2021. The effects of using magnetized water in reactive powder concrete with different curing methods. *IOP Conference Series: Materials Science and Engineering, 1067(1), P. 012017*. https://doi.org/10.1088/1757-899X/1067/1/012017

Luti, A.A. and Abbas, Z.K., 2024a. The effect of different curing methods on the properties of reactive powder concrete reinforced with various fibers. *Engineering, Technology & Applied Science Research*, 14(3), pp. 14225–14232. https://doi.org/10.48084/etasr.7072

Majeed, W.Z., Aboud, R.K., Naji, N.B., and Mohammed, S.D., 2023. Investigation of the impact of glass waste in reactive powder concrete on attenuation properties for Bremsstrahlung ray. *East European Journal of Physics*, 1, pp. 102–108. https://doi.org/10.26565/2312-4334-2023-1-12

Muhsin, Z.F. and Fawzi, N.M., 2021. Effect of fly ash on some properties of reactive powder concrete. *Journal of Engineering*, 27(11), pp. 32–46. https://doi.org/10.31026/j.eng.2021.11.03

Nafees, A., Javed, M.F., Musarat, M.A., Ali, M., Aslam, F. and Vatin, N.I., 2021. FE modelling and analysis of beam-column joint using reactive powder concrete. *Crystals*, 11(11), P. 1372. https://doi.org/10.3390/cryst11111372

Nayak, D.K., Abhilash, P.P., Singh, R., Kumar, R., and Kumar, V., 2022. Fly ash for sustainable construction: A review of fly ash concrete and its beneficial use case studies. *Cleaner Materials*, 6, P. 100143. https://doi.org/10.1016/j.clema.2022.100143

Papp, V., Ardelean, I., Bulátkó, A., László, K., Csík, A., Janovics, R., and Kéri, M., 2025. Effect of metakaolin and fly ash on the early hydration and pore structure of Portland cement. *Cement and Concrete Research, 196*, 107928. https://doi.org/10.1016/j.cemconres.2025.107928

Rahul, R., Chithra, R., and Thenmozhi, R., 2023. Experimental investigation on reactive powder concrete by partial replacement of cement with different pozzolanic materials. *International Journal for Research in Applied Science & Engineering Technology*, 11(6). https://doi.org/10.22214/ijraset.2023.54041

Richard, P. and Cheyrezy, M., 1995. Composition of reactive powder concretes. *Cement and Concrete Research*, 25(7), pp. 1501–1511. https://doi.org/10.1016/0008-8846(95)00144-2

Safitri, E., Wibowo, and Fadhil, B.D., 2024. Compressive strength study on reactive powder concrete with 30% quartz sand and variations in fly ash composition as partial substitution of cement. *Sustainable Civil Building Management and Engineering Journal*, 1(3), pp. 1–9. https://doi.org/10.47134/scbmej.v1i3.3009

Shannag, M.J., 2000. High-strength concrete containing natural pozzolan and silica fume. *Cement and Concrete Composites*, 22(6), pp. 399–406. https://doi.org/10.1016/S0958-9465(00)00037-8

Shannag, M.J. and Yeginobali, A., 1995. Properties of pastes, mortars, and concretes containing natural pozzolan. *Cement and Concrete Research*, 25(3), pp. 647–657. https://doi.org/10.1016/0008-8846(95)00053-F

Soutsos, M.N., Millard, S.G. and Karaiskos, K., 2006. Mix design, mechanical properties, and impact resistance of reactive powder concrete (RPC). In: *International RILEM Workshop on High Performance Fiber Reinforced Cementitious Composites in Structural Applications*. Champs-sur-Marne, France: RILEM Publications SARL, pp. 549–560.

Thomas, M.D.A., 2007. *Optimizing the Use of Fly Ash in Concrete*. Skokie, IL, USA: Portland Cement Association.

Xu, J., Wu, C., Xiang, H., Su, Y., Li, Z.X., Fang, Q., Hao, H., Liu, Z., Zhang, Y. and Li, J., 2016. Behaviour of ultra-high performance fibre reinforced concrete columns subjected to blast loading. *Engineering Structures*, 118, pp. 97–107. https://doi.org/10.1016/j.engstruct.2016.03.048

Yazıcı, H., Yardımcı, M.Y., Aydın, S. and Karabulut, A.S., 2009. Mechanical properties of reactive powder concrete containing mineral admixtures under different curing regimes. *Construction and Building Materials,* 23(3), pp. 1223–1231. https://doi.org/10.1016/j.conbuildmat.2008.08.003

تأثير إضافة الرماد المتطاير والمعالجة الحرارية على أداء خرسانة المساحيق الفعالة

ناديه سلمان حسين*، هديل خالد عواد

قسم الهندسة المدنية، كلية الهندسة، جامعة بغداد، بغداد، العراق

الخلاصة

تهدف هذه الدراسة إلى تقييم تأثير المعالجة الحرارية وإضافة الرماد المتطاير على الخواص الميكانيكية والفيزيائية للخرسانة المسحوقة الفعالة(RPC) ، بهدف تطوير خلطة أكثر استدامة من خلال الاستبدال الجزئي للإسمنت البورتلاندي الاعتيادي (OPC)بالرماد المتطاير. تم تحضير أربع خلطات، شملت خلطة مرجعية (R) وخلطات تحتوي على نسب استبدال من الرماد المتطاير مقدارها 10% و20% و30%، ورُمز لها بـ RF10 و RF20و RF30على التوالي. تم صب ثلاث نماذج لكل خلطة ولكل عمر فحص. عُرضت النماذج إلى معالجة حرارية عند درجة حرارة 70°م لمدة 5 ساعات يوميًا ولمدة ثلاثة أيام، تلتها المعالجة بالماء حتى موعد الفحص .أظهرت النتائج أن إضافة 20% من الرماد المتطاير حسّنت الأداء الكلي للخرسانة المسحوقية الفعّالة. إذ حققت خلطة RF20 أفضل مقاومة انضغاط، بزيادات بلغت 3.39% و4.47% و4.86% عند أعمار 7 و28 و56 يومًا على التوالي مقارنة بالخلطة المرجعية. علاوة على ذلك، ازدادت مقاومة الانثناء ومقاومة الشد الانشطاري بنسبة 2.39% و1.69% على التوالي عند عمر 28 يومًا. كما سجلت خلطة RF20 أعلى كثافة جافة بلغت 2683 كغم/م^3، وأقل امتصاص للماء بنسبة 0.114%، وأقل مسامية بنسبة 1.75%. ومع ذلك، أدى استبدال 30% من الإسمنت بالرماد المتطاير إلى انخفاض الخواص الميكانيكية. وأشارت النتائج إلى أن إضافة 20% من الرماد المتطاير تحت ظروف المعالجة الحرارية يمكن أن تُحسن أداء الخرسانة المسحوقية الفعّالة بصورة فعّالة، فضلًا عن تعزيز الاستدامة من خلال تقليل استهلاك الإسمنت.

الكلمات المفتاحية: الخرسانة المسحوقة التفاعلية، الرماد المتطاير، الألياف الفولاذية، الخصائص الميكانيكية، المعالجة الحرارية، نظام المعالجة.